Journal of Power Sources 239 (2013) 181–188

Contents lists available at SciVerse ScienceDirect

Journal of Power Sources

journal homepage: www.elsevier.com/locate/jpowsour

Enhanced electrochemical performances of 5 V spinel $LiMn_{1.58}Ni_{0.42}O_4$ cathode materials by coating with $LiAlO_2$

Fuquan Cheng, Yuelong Xin, Youyuan Huang, Jitao Chen, Henghui Zhou*, Xinxiang Zhang

College of Chemistry and Molecular Engineering, Peking University, Beijing 100871, PR China

HIGHLIGHTS

- $LiAlO_2$-surface modified $LiMn_{1.58}Ni_{0.42}O_4$was prepared from Al_2O_3-coated $Mn_{0.79}Ni_{0.21}CO_3$ precursor.
- $LiAlO_2$ modification enhances the rate capability and cyclability of $LiMn_{1.58}Ni_{0.42}O_4$.
- $LiAlO_2$ modification stabilizes the electrode/electrolyte interface.

ARTICLE INFO

Article history:
Received 9 February 2013
Received in revised form
24 March 2013
Accepted 25 March 2013
Available online 3 April 2013

Keywords:
Lithium ion batteries
Spinel cathode oxides
Lithium aluminate coating
Surface modification

ABSTRACT

$LiAlO_2$-surface modified $LiMn_{1.58}Ni_{0.42}O_4$ spinel cathode materials have been prepared by coating Al_2O_3 on $Mn_{0.79}Ni_{0.21}CO_3$ precursors, followed by post-sintering with Li_2CO_3 at 900 °C. X-ray diffraction and FT-IR analyses indicate that during the calcination process aluminum ions not only react with Li_2CO_3 to form a strengthened $LiAlO_2$ coating layer but also migrate from the surface into the spherical particles. The $LiAlO_2$-surface modified $LiMn_{1.58}Ni_{0.42}O_4$ samples exhibit excellent electrochemical performance compared to that of the bare one in terms of rate capability and cyclability. In particular, the 1 mol.% $LiAlO_2$-surface modified sample can deliver a discharge capacity of 100.6 m Ah g^{-1} even at a high current density of 4 C-rate, while the bare one only has a discharge capacity of 49.5 m Ah g^{-1}. At 55 °C, the 1 mol.% $LiAlO_2$-surface modified $LiMn_{1.58}Ni_{0.42}O_4$ sample shows outstanding cyclability with less than 5% capacity fade after 150 cycles. Based on these results, coating on the precursors to prepare a strengthened $LiAlO_2$ coating layer would be a promising method to enhance the electrochemical performance of 5 V spinel cathode materials.

© 2013 Elsevier B.V. All rights reserved.

1. Introduction

Rechargeable lithium-ion batteries have enabled the wireless revolution of portable electronic devices and exhibit great prospect for the large-scale application in the field of electric vehicles and smart grid. Unfortunately, the currently commercial cathode material, $LiCoO_2$, is hard to the meet the requirements of large-scale application due to its limited energy density, high cost, and toxicity. Development of alternative cathode materials with high energy density and low cost is critical for next generation high-energy lithium-ion batteries [1–3]. In this regard, spinel $LiMn_{2-x}Ni_xO_4$ ($0 < x \leq 0.5$) cathode oxides are attractive as they have a high operating voltage of ~4.7 V vs. Li^+/Li and a theoretical capacity of 147 m Ah g^{-1} (equivalent to an energy density of 600 Wh kg^{-1}) [4–11].

However, at the high operating voltage of ~4.7 V, the decomposition of electrolyte aggravates and a thick solid-electrolyte interphase (SEI) layer with poor electronic and lithium conductivity is formed on the electrode surface [12–15]. As a result, 5 V spinel cathode oxides undergo severe capacity fade, particularly at elevated temperatures. To suppress the undesired side-reactions, coating with an inert material, such as Al_2O_3, ZnO, MPO_4 (M = Fe, Ni), and ZrO_2, has been developed, leading to improved electrochemical performances [16–20]. For instance, the 1 wt. % $FePO_4$-modified $LiMn_{1.5}Ni_{0.5}O_4$ cathode material reported by Liu et al. exhibits outstanding cyclability with capacity retention of 99.3% after 50 cycles, whereas the bare sample exhibits 21% capacity fade [20]. However, these inert coating materials are usually poor conductors of lithium and electron and are also weakly bonded to the parent material owing to the low post-sintering temperature. Recently, a strengthened lithium-containing coating layer, prepared by coating on the precursors with metal oxides and sintering with Li_2CO_3 subsequently, has been developed to improve the electrochemical performances of layered $LiMO_2$ (M = Ni, Co, Mn,

* Corresponding author. Tel./fax: +86 10 62757908.
E-mail address: hhzhou@pku.edu.cn (H. Zhou).

0378-7753/$ – see front matter © 2013 Elsevier B.V. All rights reserved.
http://dx.doi.org/10.1016/j.jpowsour.2013.03.143

et al.) cathode materials [21–23]. Inspired by these findings, we report herein a $LiAlO_2$ coating layer to enhance the electrochemical performances of $LiMn_{1.58}Ni_{0.42}O_4$ spinel cathode oxides. The $LiAlO_2$-surface modified $LiMn_{1.58}Ni_{0.42}O_4$ samples were prepared by a two-step strategy that involves coating Al_2O_3 on the spherical $Mn_{0.79}Ni_{0.21}CO_3$ precursors and subsequent post-calcination with Li_2CO_3 at 900 °C in air, as illustrated in Scheme 1.

2. Experimental

The bare $LiMn_{1.58}Ni_{0.42}O_4$ sample was synthesized by a solid-state reaction of Li_2CO_3 and $Mn_{0.79}Ni_{0.21}CO_3$ at 900 °C for 15 h. The $Mn_{0.79}Ni_{0.21}CO_3$ carbonate precursors were prepared by a co-precipitation method. In a typical reaction, the appropriate amounts of transition metals sulfates were dissolved into deionized water and then were added into a tank reactor drop by drop. Meanwhile, sodium carbonate and ammonia solutions were separately feed into the tank reactor. The precipitated $Mn_{0.79}Ni_{0.21}CO_3$ carbonate precursors were washed with deionized water several times and then were dried in an air oven at 100 °C for 24 h.

To prepare Al_2O_3 surface modified $LiMn_{1.58}Ni_{0.42}O_4$ sample, aluminum isopropoxide was dissolved in ethanol, and then the above-synthesized $Mn_{0.79}Ni_{0.21}CO_3$ precursor was dispersed into the solution. The Al content was set at molar ratios of Al/(Ni + Mn) = 0.5, 1, 2, and 5% by controlling the amount of aluminum isopropoxide. The suspension was heated at 80 °C to evaporate ethanol, and the dried powder was calcinated at 420 °C for 5 h to remove water. The obtained composite was mixed with Li_2CO_3 thoroughly and then was sintered at 900 °C for 15 h in air.

The XRD data were recorded on a Rigaku X-ray diffractometer equipped with Cu Kα radiation. The morphologies of these materials were analyzed with a FEI Quanta 200FEG environmental scanning electron microscopy (ESEM) and a FEI F20 transmission electron microscopy (TEM). The Li, Mn, and Ni content in the final spinel oxides was analyzed using an inductively coupled plasma-atomic emission spectrometer (ICP-AES). FTIR spectra were collected with KBr pellets with a Bruker IR spectrometer. The KBr pellets were prepared by diluting a minute amount of cathode oxide powder in 100 mg of KBr powder and pressing at a pressure of 10 MPa subsequently. Each IR spectrum was an average of 32 scans taken between 700 and 400 cm^{-1} with a spectral resolution of 4 cm^{-1}. Cathode electrodes were prepared by spreading slurry consisting of 80 wt.% active material, 10 wt.% Super P carbon, and 10 wt.% polyvinylidene fluoride on aluminum foils by a doctor-blade method. CR2032 coin cells were assembled in an Argon-filled glove box with the as-prepared cathode electrodes, lithium metallic anode, and 1.0 mol L^{-1} $LiPF_6$ in ethylene carbonate/diethyl carbonate (1:1 by volume) electrolyte. Electrochemical performances were evaluated with CR2032 coin-cells on a Land CT2001A battery cycler. Electrochemical impedance spectroscopy (EIS) data of the cycled cells were collected in a frequency range from 100 kHz to 0.01 Hz with an ac amplitude of 5 mV amplitude on an Autolab electrochemical work station. Before the EIS measurements, all the cells were charged to 50% state of charge (SOC) and then rested for 1 h at room temperature to relax the cell potential to a stable open-circuit voltage value.

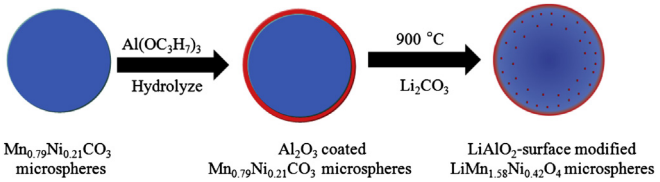

Scheme 1. Two-step approach for the preparation of $LiAlO_2$-surface modified $LiMn_{1.58}Ni_{0.42}O_4$ microspheres.

3. Results and discussion

Fig. 1 shows the typical SEM images of the bare and coated $Mn_{0.79}Ni_{0.21}CO_3$ carbonate precursors with 0.25, 0.5, 1, and 2.5 mol.% of Al_2O_3. The uncoated precursor exists as monodisperse spherical secondary particles with an average diameter of about

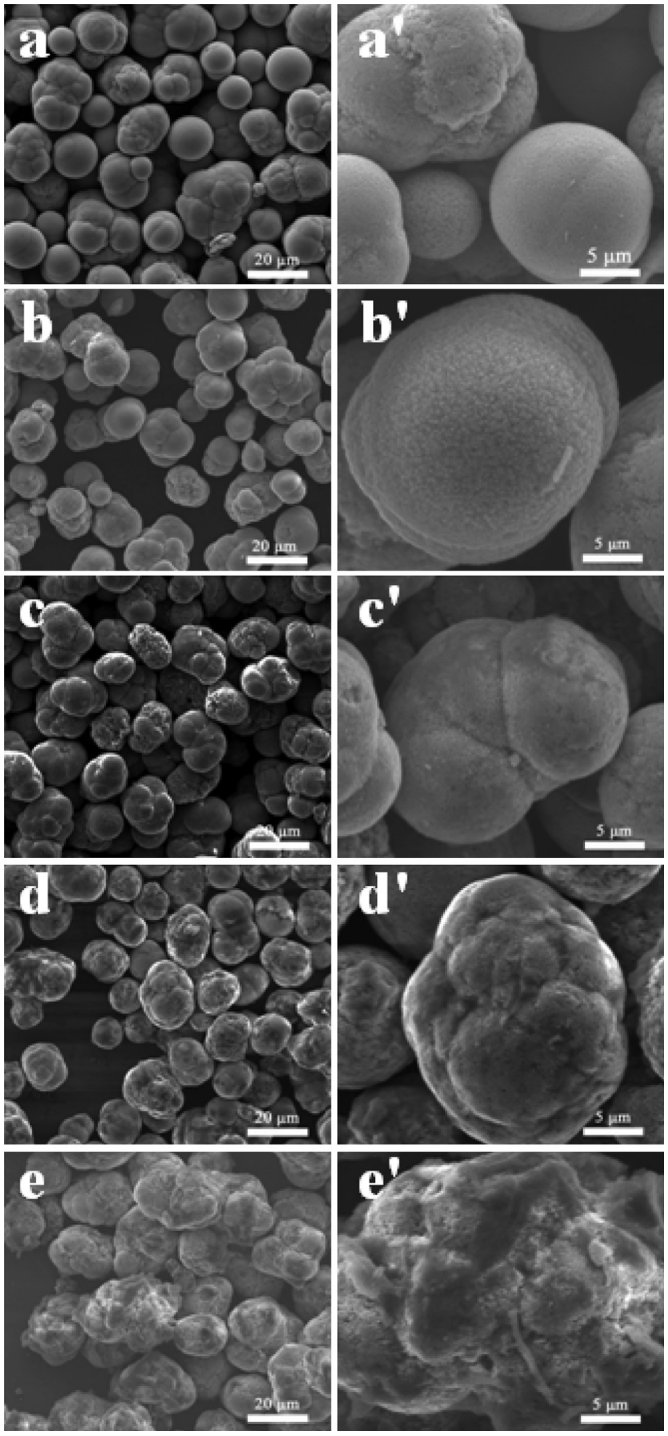

Fig. 1. Typical SEM images of the bare (a) and Al_2O_3-coated $Mn_{0.79}Ni_{0.21}CO_3$ precursors with different molar ratio: (b) 0.25 mol.%, (c) 0.5 mol.%, (d) 1 mol.%, and (e) 2.5 mol.%. The corresponding magnified SEM images are shown in (a'–e').

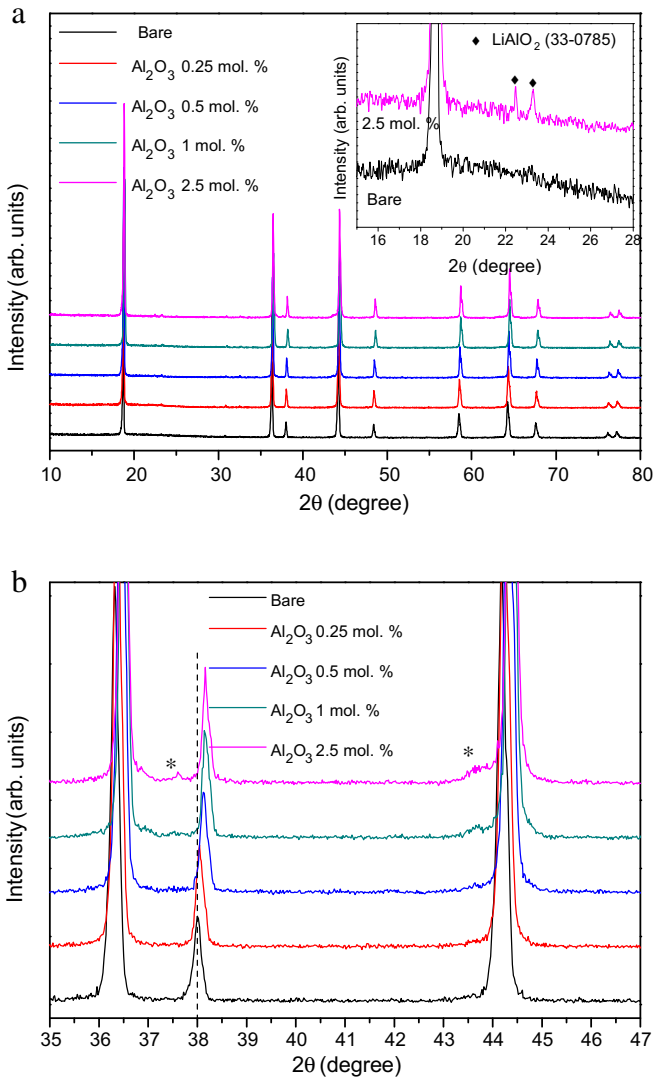

Fig. 2. (a) X-ray diffraction patterns of the bare and $LiAlO_2$-surface modified spinel $LiMn_{0.58}Ni_{0.42}O_2$ oxides. (b) The corresponding magnified XRD patterns in the 2θ range of 35–47°, showing the peak shift and the evolution of the $Li_{1-z}Ni_zO$ oxide.

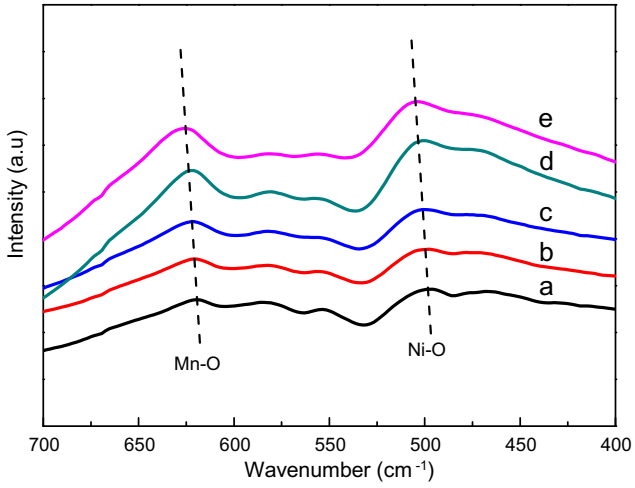

Fig. 3. FI-IR spectra of the bare (a) and $LiAlO_2$-surface modified $LiNi_{0.42}Mn_{1.58}O_4$ with different molar ratio: (b) 0.5 mol.%, (c) 1 mol.%, (d) 2 mol.%, (e) 5 mol.%.

15 μm (Fig. 1a). A close observation reveals that the spherical secondary particles are actually built up by nanoparticles (Fig. 1a'). It is clear that the uncoated one has a clean and smooth surface, so with the 0.25 mol.% Al_2O_3 coated $Mn_{0.79}Ni_{0.21}CO_3$ (Fig. 1b). As the amount of Al_2O_3 coating increases to 0.5 mol.%, a thin and uniform Al_2O_3 coating layer can be observed on the surface of the spherical secondary particles. Further increasing the Al_2O_3 coating content leads to thick and uneven coating layers, as shown in Fig. 1d and e. In addition, the SEM images of the Al_2O_3-coated $Mn_{0.79}Ni_{0.21}CO_3$

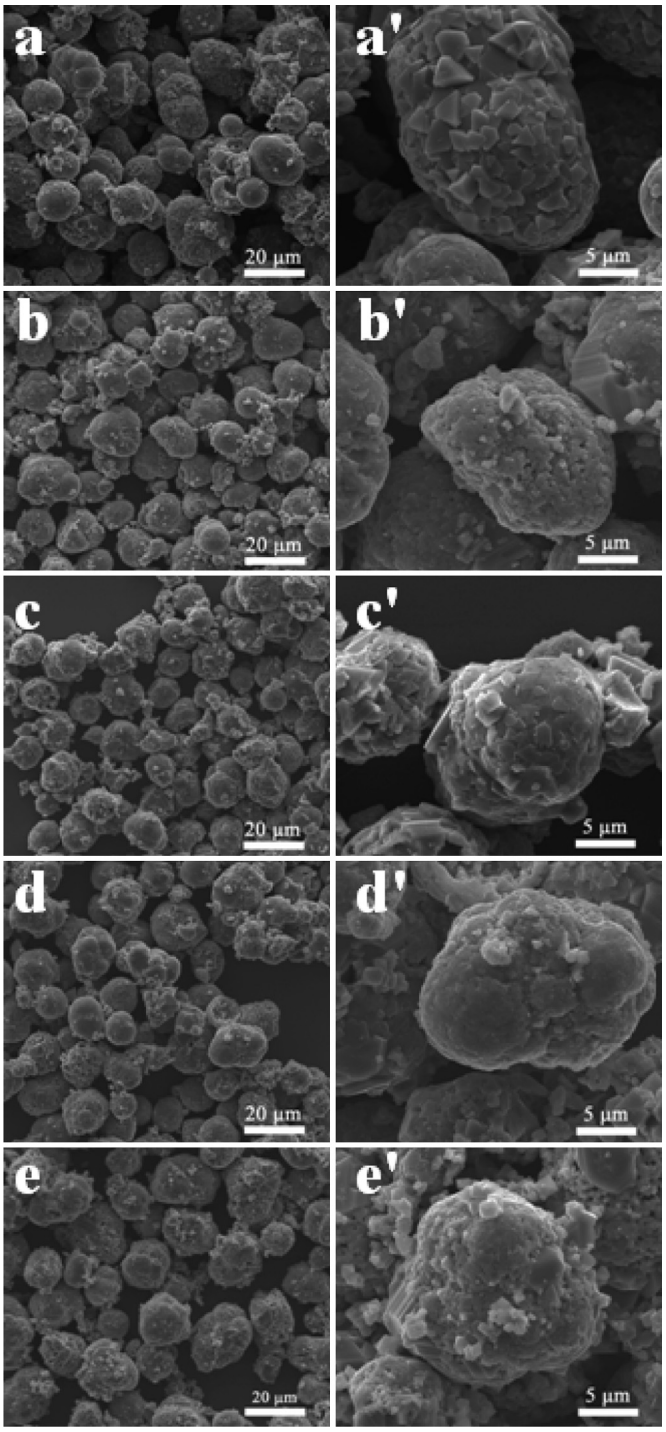

Fig. 4. Typical SEM images of the bare (a) and $LiAlO_2$-surface modified $LiMn_{1.58}Ni_{0.42}O_4$ samples with different molar ratio: (b) 0.5 mol.%, (c) 1 mol.%, (d) 2 mol.%, (e) 5 mol.%. The corresponding magnified SEM images are shown in (a'–e').

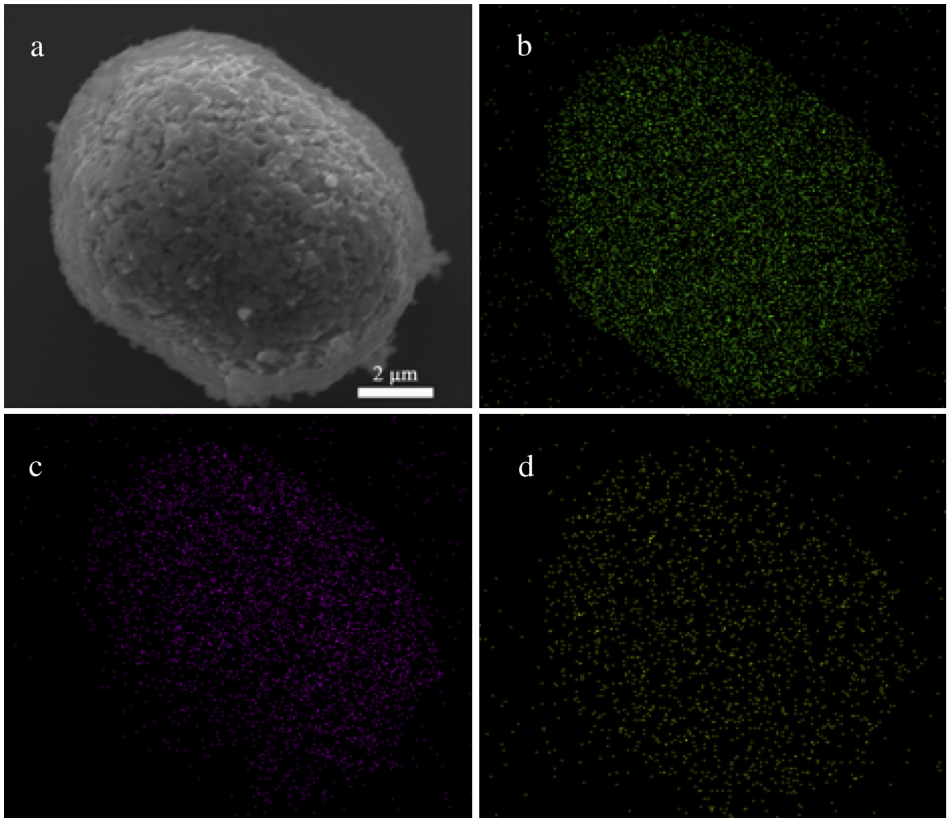

Fig. 5. EDX mappings of 1 mol.% $LiAlO_2$-surface modified $LiMn_{1.58}Ni_{0.42}O_4$ sample (a), Mn (b), Ni (c), and Al (d).

carbonate precursors become fuzzy as the molar ratio of Al_2O_3 coating increases, which may arise from the poor electronic conductivity of the Al_2O_3 coating layer [24].

Further sintering the bare and Al_2O_3-coated $Mn_{0.79}Ni_{0.21}CO_3$ carbonate precursors with Li_2CO_3 at 900 °C in air produces the final spinel $LiMn_{1.58}Ni_{0.42}O_4$ cathode oxides. The contents of metal ions in the prepared $LiMn_{1.58}Ni_{0.42}O_4$ spinel oxides were analyzed by a ICP-AES method. The experimental molar ratio of the Li: Mn: Ni in all the samples is about 1.00: 1.58: 0.42, in a good agreement with the nominal value in the spinel $LiMn_{1.58}Ni_{0.42}O_4$ cathode oxide. Fig. 2 compares the X-ray diffraction patterns of the bare and surface modified $LiMn_{1.58}Ni_{0.42}O_4$ samples. All these samples exhibit similar diffraction patterns, which can be indexed in a cubic spinel structure with the *Fd*-3*m* space group [4,25,26]. In this cubic structure, lithium ions reside at the 8a tetrahedral sites and transition metal ions of Ni and Mn occupy 16d octahedral sites [26]. Notably, the magnified XRD pattern of the 2.5 mol.% Al_2O_3-coated sample (inset of Fig. 3a) shows two weak diffraction peaks at around 22–24°, which can be identified as the $LiAlO_2$ phase (JCPDS 33-0785). The appearance of the $LiAlO_2$ phase confirms the reaction of Al_2O_3 coating layer with Li_2CO_3 during the calcination process. Based on this result, it is reasonable to speculate that the Al_2O_3 coating layer in other samples with lower

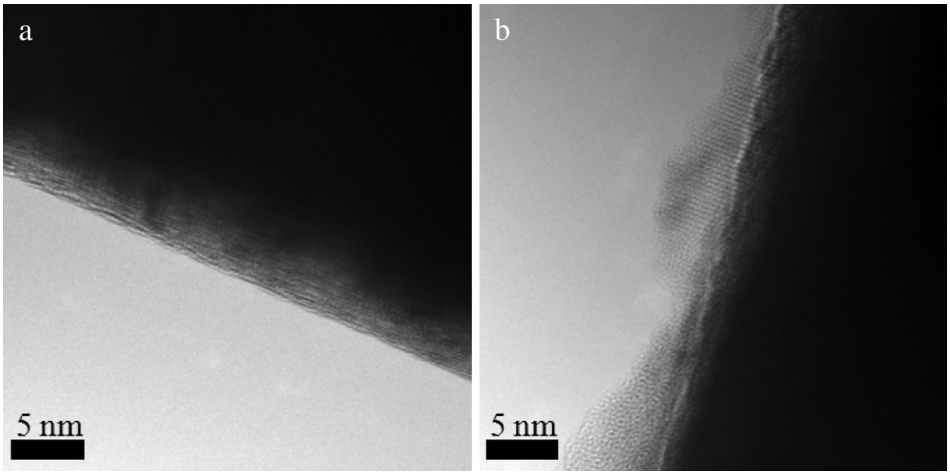

Fig. 6. Typical TEM images of bare (a) and 1 mol.% $LiAlO_2$-surface modified $LiMn_{1.58}Ni_{0.42}O_4$ samples (b).

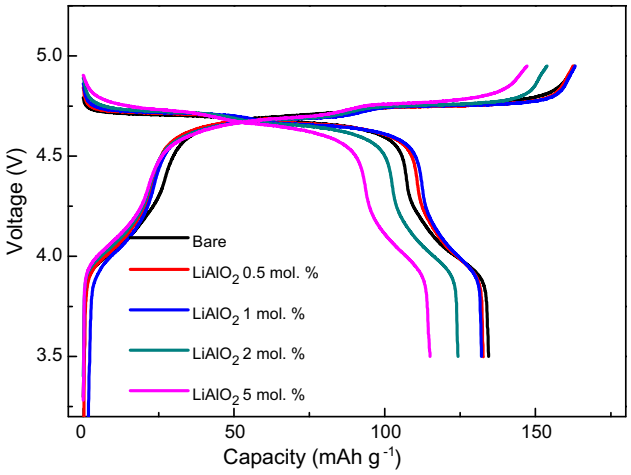

Fig. 7. First cycle charge and discharge curves of the bare and $LiAlO_2$-surface modified $LiMn_{1.58}Ni_{0.42}O_4$ samples.

Al_2O_3 content (i.e., 0.5, 1, and 2 mol.%) also transforms into the $LiAlO_2$ phase, though it is undetectable by XRD technique. Therefore, we denote these final spinel cathode oxides as $LiAlO_2$-surface modified $LiMn_{1.58}Ni_{0.42}O_4$ samples henceforward.

More importantly, the positions of X-ray diffraction peaks progressively shift toward higher angles with increasing amount of $LiAlO_2$ coating (Fig. 2b), indicating the decrease of the lattice parameter. In particular, the lattice parameter of the cubic structure decreases from 8.193 Å for the uncoated one to 8.164 Å for the surface modified sample with 5 mol.% $LiAlO_2$. The gradual decrease of the lattice parameter with increasing amount of $LiAlO_2$ coating can be attributed to the substitution of transition metal ions by smaller-sized Al^{3+} ions (0.054 nm) based on previous studies [27,28]. This result indicates that Al^{3+} ions in the coating layer not only react with Li_2CO_3 to form the $LiAlO_2$ phase but also diffuse toward the interior of spherical particles during the calcination process. Notably, diffraction peaks at ~37° and 43° appear in the modified $LiMn_{1.58}Ni_{0.42}O_4$ sample with 2 mol.% of $LiAlO_2$, and these two peaks become distinct as the content of $LiAlO_2$ coating increases to 2.5 mol.%. According to previous studies, these two diffraction peaks can be attributed to the $Li_zNi_{1-z}O$ impurity phase [4,6,7]. The formation of this impurity phase implies a decrease in the Ni/Mn ratio in the spinel phase, as suggest by the EDS Analysis in an early report [7].

To further confirm the incorporation of Al^{3+} ions into the spinel structure, we analyze the local environment of cations in the spinel phase by utilization of FT-IR technique. Fig. 3 compares the FT-IR spectra of the bare $LiMn_{1.58}Ni_{0.42}O_4$ and surface modified $LiMn_{1.58}Ni_{0.42}O_4$ samples with 0.5, 1, 2, and 5 mol.% of $LiAlO_2$. All these samples show five distinct absorption bands, in good agreement with those reported in literature [25,29]. On the basis of previous studies [25], the adsorptions at ~500 cm^{-1} and ~620 cm^{-1} are ascribed to the asymmetric stretching modes of Ni–O bond and Mn–O bond, respectively. Clearly, both the Ni–O and Mn–O bonds show a gradual blue shift. In particular, the wavenumber of Ni–O bond shifts from 498 cm^{-1} for the bare one to 503 cm^{-1} for the modified sample with 5 mol.% $LiAlO_2$, whereas that of the Mn–O bond changes from 619 cm^{-1} to 625 cm^{-1}. The blue shift of Mn–O and Ni–O bonds arises from the incorporation of aluminum ions that have lower atomic mass and higher electronegativity than manganese and nickel ions into the spinel structure [30]. This result provides further proof that Al^{3+} ions migrate from surface into the spinel structure during the calcination process.

Fig. 4 shows the typical SEM images of the bare $LiMn_{1.58}Ni_{0.42}O_4$ and surface modified $LiMn_{1.58}Ni_{0.42}O_4$ samples with 0.5, 1, 2, and 5 mol.% of $LiAlO_2$. After sintering with Li_2CO_3 at 900 °C, all of these samples still maintain the spherical shape with the diameter almost as the same as that of the carbonate precursor. However, the morphology of primary particles transits from nanoparticles into microsized-polyhedral particles because of the heat treatment and the addition of Li^+ ions into the structure. With increasing amount of $LiAlO_2$ coating, the surface of the spherical secondary particles becomes more smoother owing to the formation of the strengthened $LiAlO_2$ coating layer during the calcination process. To investigate the elemental distribution on the surface of spherical secondary particles, energy dispersive X-Ray (EDX) mapping for Mn, Ni, and Al was carried out, and the result is shown in Fig. 5. According to Fig. 5, Al element distributes evenly on the surface of the 1 mol.% $LiAlO_2$-modified $LiMn_{1.58}Ni_{0.42}O_4$ particles, indicating that the prepared spinel cathode oxides are uniformly coated with $LiAlO_2$. TEM bright-field images in Fig. 6 further confirm that the surface of $LiAlO_2$-modifed $LiMn_{1.58}Ni_{0.42}O_4$ sample is completely enwrapped by a $LiAlO_2$ coating layer with a thickness of about 5 nm, whereas the bare one has a clean surface.

Electrodes containing the final spinel cathode oxides were fabricated and evaluated in 2032-type coin cells with metal lithium anode. Fig. 7 compares the first cycle charge and discharge voltage profiles of the bare $LiMn_{1.58}Ni_{0.42}O_4$ and surface modified $LiMn_{1.58}Ni_{0.42}O_4$ samples with 0.5, 1, 2, and 5 mol.% of $LiAlO_2$ in the

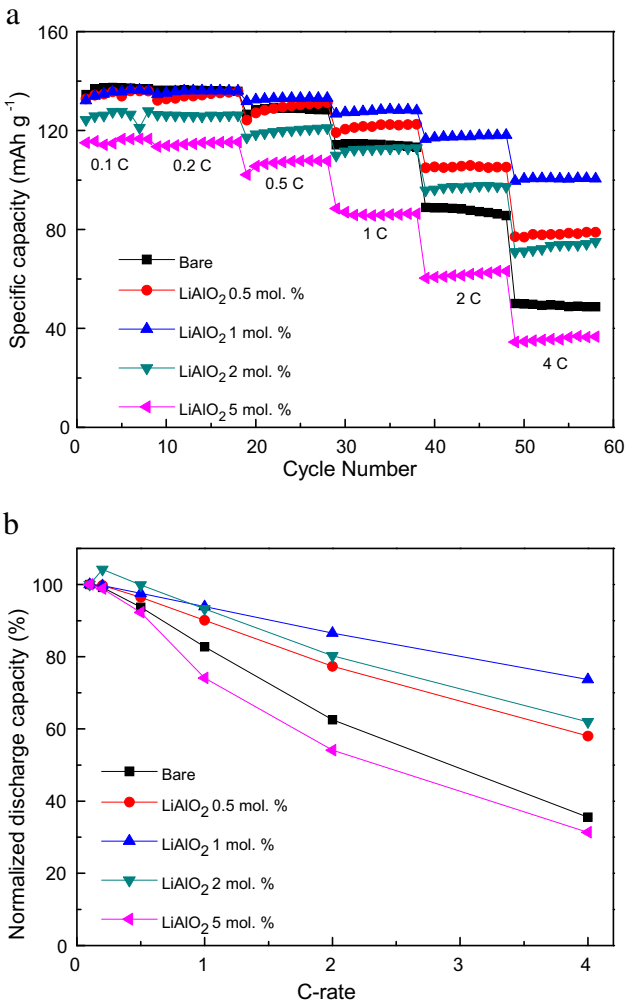

Fig. 8. (a) Rate capabilities of the bare and $LiAlO_2$-surface modified $LiMn_{1.58}Ni_{0.42}O_4$ samples between 3.5 and 5 V at 0.1 C, 0.1 C, 0.5 C, 2 C, and 4 C-rate. (b) Variation of normalized discharge capacity with C-rates.

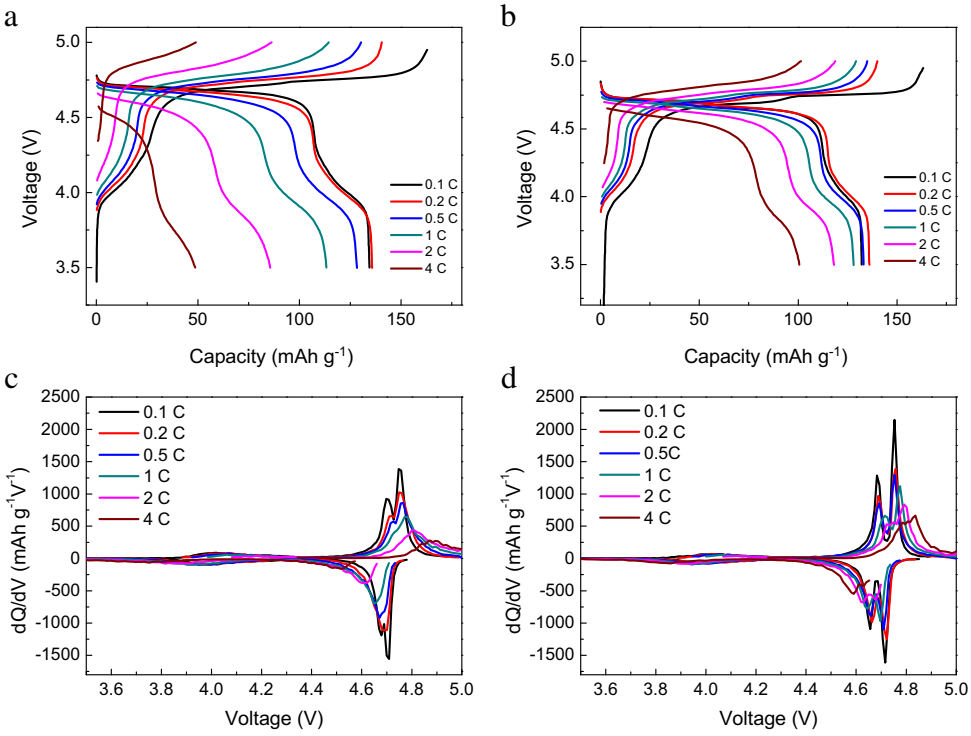

Fig. 9. Charge and discharge profiles at 0.1 C, 0.1 C, 0.5 C, 2 C, and 4 C-rate of the bare (a) and 1 mol.% $LiAlO_2$-surface modified $LiMn_{1.58}Ni_{0.42}O_4$ samples (b). The corresponding *dQ/dV* curves are shown in (c) and (d), respectively.

voltage range of 3.5–5.0 V at 0.1 C-rate. All of these samples exhibit similar voltage capacity profiles with three distinct plateaus: two stepwise plateaus at ~4.7 V, corresponding to the Ni^{2+}/Ni^{3+} and Ni^{3+}/Ni^{4+} redox couples, and one plateau at ~4 V, arising from the Mn^{3+}/Mn^{4+} redox couple [4,5,31]. This result demonstrates that the $LiAlO_2$ surface modification does not change the intrinsic charge and discharge behaviors of $LiMn_{1.58}Ni_{0.42}O_4$ spinel cathode oxides. The bare sample delivers a high discharge capacity of 134.5 m Ah g^{-1}. After surface modification with 0.5 mol.% and 1 mol.% $LiAlO_2$, the discharge capacity does not show significant degradation. Further increasing the amount of the $LiAlO_2$ coating, however, leads to a severe irreversible capacity loss. Particularly, the initial discharge capacities of the 2 mol.% and 5 mol.% $LiAlO_2$-surface modified samples are, respectively, 124.3

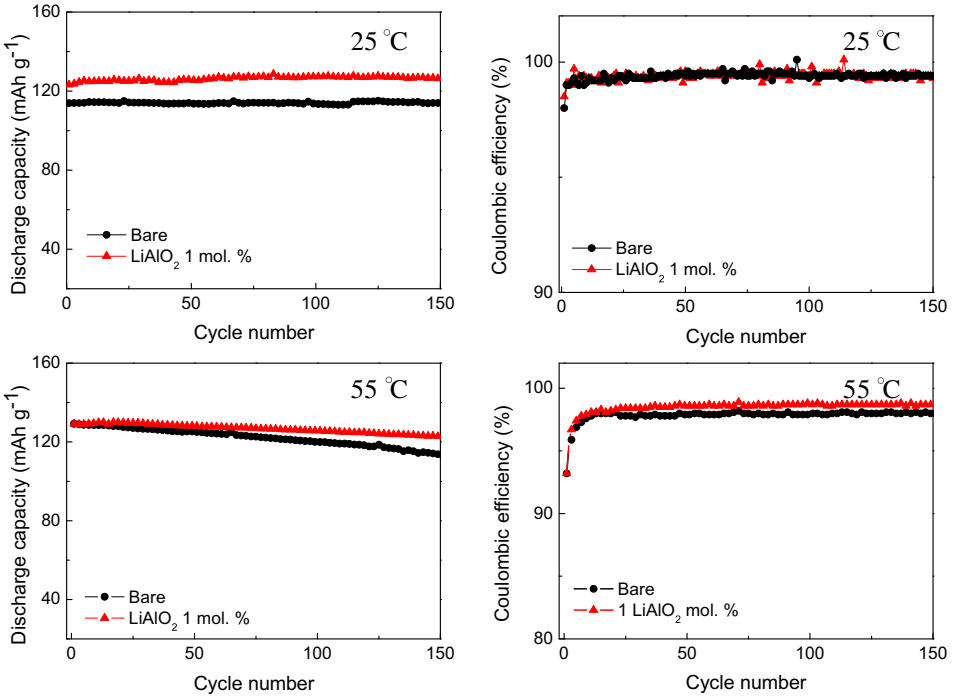

Fig. 10. Cyclability and Coulombic efficiency of the bare and 1 mol.% $LiAlO_2$-surface modified $LiMn_{1.58}Ni_{0.42}O_4$ samples at 25 °C and 55 °C.

and 115.0 m Ah g^{-1}, which are much smaller than that of the uncoated one. This irreversible capacity loss is closely related to the amount of $LiAlO_2$ coating used. The $LiAlO_2$ coating layer is an electrochemical inactive material, which will significantly decrease the content of electrochemical active material in the final electrodes when large amount of $LiAlO_2$ coating is used, resulting in the observed reversible capacity loss. In addition, the $Li_zNi_{1-z}O$ impurity phase in the 5 mol.% $LiAlO_2$-surface modified sample reduces the electrochemical active nickel ions in the spinel phase [7], which may also contribute to the irreversible capacity loss.

Fig. 8a shows the rate capability of bare and $LiAlO_2$-surface modified $LiMn_{1.58}Ni_{0.42}O_4$ samples. The rate capability was evaluated by charging and discharging galvanostatically at the same current density from 0.1 C to 4 C rate for ten cycles per step. The $LiAlO_2$-surface modified samples exhibit enhanced rate capability compared to that of the bare sample, except the one with 5 mol.% $LiAlO_2$ coating. Among these surface modified samples, the one with 1 mol.% $LiAlO_2$ coating exhibits the best rate capability. In particular, the 1 mol.% $LiAlO_2$-surface modified sample delivers a discharge capacity of 100.6 m Ah g^{-1} at 4 C-rate, while the bare one only has a discharge capacity of 49.5 m Ah g^{-1}. In other words, the 1 mol.% $LiAlO_2$-surface modified sample maintains 75.6% of its capacity at 4 C-rate, which is about two times of the bare sample (Fig. 8b).

To further understand the enhanced rate capability of $LiAlO_2$-surface modified samples, Fig. 9a and b compare the charge and discharge curves of the bare sample and the 1 mol.% $LiAlO_2$-surface modified sample. As the tested current density increases, the charge curves of both samples move to higher potential whereas the discharge curves shift toward lower potential, accompanied by a gradual degradation of reversible capacities. This polarization behavior is much more obvious in the corresponding differential-capacity (dQ/dV) curves, as shown in Fig. 9c and d. When the current density increases, the oxidation peaks move to high voltage region, whereas the reduction peaks move to low voltage region. As a result, the separation between the oxidation peak and the reduction peak increases with increasing current densities. However, at the same current density used, the peak separation of the $LiAlO_2$-surface modified sample is much smaller than that of the uncoated one. Moreover, even under a high current density of 2 C-rate, the two oxidation (or reduction) peaks at ~4.7 V in the dQ/dV curves of the $LiAlO_2$-surface modified sample are still well-separated, while the double peaks in the bare one overlap into a broad peak. These results indicate that the $LiAlO_2$ surface modification can significantly decrease the polarization, leading to the high capacity retention under large current density.

Fig. 10 compares the cyclability of the bare $LiMn_{1.58}Ni_{0.42}O_4$ and surface modified $LiMn_{1.58}Ni_{0.42}O_4$ with 1 mol.% of $LiAlO_2$. The cycling test was carried out separately at 25 °C and 55 °C at 1 C-rate for 150 cycles. At 25 °C, both these two samples exhibit excellent cyclability during the first 150 cycles with the Coulombic efficiency near 100%. However, at 55 °C, the bare sample exhibits gradually capacity fade upon cycling with 12% capacity loss after 150 cycles, and the average Coulombic efficiency is only about 97.9%. After $LiAlO_2$ surface modification, the final cathode electrode shows less than 5% capacity fade after 150 cycles, much lower than that of the bare electrode, and the average Coulombic efficiency increases to about 98.6%. It is well recognized that the poor cycling performance of the 5 V spinel cathodes at 55 °C is mainly caused by the aggressive side-reactions between the cathode and the electrolyte at the high operating voltage up to 4.7 V [13,19]. The improved cyclability and higher Coulombic efficiency of the $LiAlO_2$-surface modified sample at 55 °C are due to the good surface protection from the strengthened $LiAlO_2$ coating layer, which suppresses the undesirable reactions between the cathode and the electrolyte.

To have a better understanding of the enhanced electrochemical performances by the $LiAlO_2$-surface modification, we performed electrochemical impedance spectroscopy (EIS) studies of the cells after 50 cycles at 25 °C and 55 °C. Fig. 11 compares the EIS plots of the bare and 1 mol.% $LiAlO_2$-surface modified samples. Each spectrum shows two semicircles. According to previous studies [13,19], the former semicircle at the high frequency region is attributed to lithium ion diffusion across the surface film on the active material, whereas the second semicircle at the medium to low frequency region is assigned to the charge transfer reaction. Based on this mechanism, the surface film resistance R_{sf} and charge transfer resistance R_{ct} can be evaluated by calculating the diameters of these two semicircles, and the results are listed in Table 1. The values of R_{sf} and R_{ct} of the bare sample are much larger than that of the $LiAlO_2$-surface modified sample, especially at 55 °C. In particular, the R_{sf} and R_{ct} of the bare sample after 50 cycles at 55 °C are, respectively, 1.04 Ohm g and 0.35 Ohm g, whereas the R_{sf} and R_{ct} of the $LiAlO_2$-surface modified

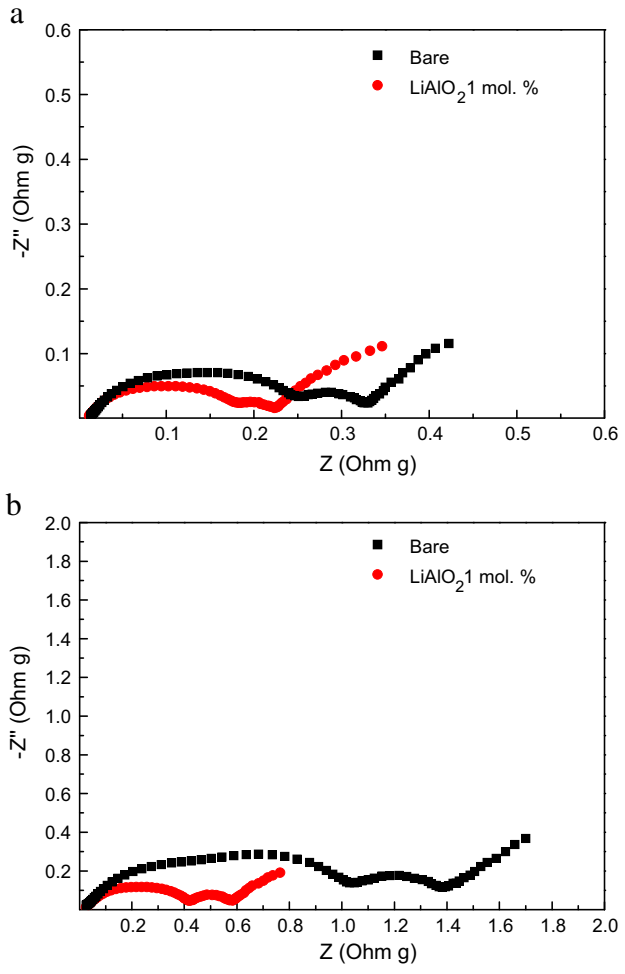

Fig. 11. Electrochemical impedance spectra (EIS) of the bare and 1 mol.% $LiAlO_2$-surface modified $LiMn_{1.58}Ni_{0.42}O_4$ samples cycled at 25 °C (a) and 55 °C (b).

Table 1
Calculated surface resistance (R_{sf}) and charge transfer resistance (R_{ct}) values of the bare and $LiAlO_2$-surface modified samples cycled at 25 °C and 55 °C.

Temperature	Bare		$LiAlO_2$-modified	
	$LiMn_{1.58}Ni_{0.42}O_4$		$LiMn_{1.58}Ni_{0.42}O_4$	
	R_{sf} (Ohm g)	R_{ct} (Ohm g)	R_{sf} (Ohm g)	R_{ct} (Ohm g)
25 °C	0.24	0.08	0.18	0.05
55 °C	1.04	0.35	0.42	0.16

sample are only 0.42 Ohm g and 0.16 Ohm g, respectively. Compared to the bare sample, the much smaller R_{sf} and R_{ct} resistances of the $LiAlO_2$-surface modified sample clearly indicate that the $LiAlO_2$-surface modification can effectively inhibit the side-reactions on the cathode surface at high voltage and high temperature and reduce the barrier for lithium ion transfer at the electrode–electrolyte interface. Therefore, the stabilized cathode surface by the $LiAlO_2$-surface modification leads to the high-rate capability and excellent cyclability.

4. Conclusion

In conclusion, a two-step procedure that involves coating Al_2O_3 on carbonate precursors and the subsequent high temperature calcinations with Li_2CO_3 has been used to fabricate $LiAlO_2$-surface modified $LiMn_{1.58}Ni_{0.42}O_4$ spinel cathode materials for lithium-ion batteries. The $LiAlO_2$-surface modified $LiMn_{1.58}Ni_{0.42}O_4$ spinel cathode oxides exhibit a gradual decrease of lattice parameter and a progressive blue shift of FT-IR spectra because part of Al^{3+} ions migrate from the surface into the spinel structure during the calcination process. As a result, a strengthened $LiAlO_2$ coating layer is formed on the surface of spherical $LiMn_{1.58}Ni_{0.42}O_4$ spinel cathode oxides, which can provide a stable interface between the electrode and the electrolyte. Finally, the $LiAlO_2$-surface modified $LiMn_{1.58}Ni_{0.42}O_4$ spinel cathode materials show excellent electrochemical performance, particularly the rate capability and cyclability. The results with the strengthened $LiAlO_2$ coating layer demonstrate a simple and effective strategy to enhance the electrochemical performance of 5 V spinel cathode oxides for high-energy lithium-ion batteries.

Acknowledgements

We appreciate support from A*Star Singapore–China Joint Research Program (No. 2012DFG52130) and the National High-Tech Research and Development Program of China (No. 2009AA035201).

References

[1] J.B. Goodenough, K.-S. Park, J. Am. Chem. Soc. (2013) 1167–1176.
[2] M.M. Thackeray, C. Wolverton, E.D. Isaacs, Energy Environ. Sci. 5 (2012) 7854–7863.
[3] B.C. Melot, J.M. Tarascon, Acc. Chem. Res. (2013), http://dx.doi.org/10.1021/ar300088q.
[4] Q.M. Zhong, A. Bonakdarpour, M.J. Zhang, Y. Gao, J.R. Dahn, J. Electrochem. Soc. 144 (1997) 205–213.
[5] H. Kawai, M. Nagata, H. Tukamoto, A.R. West, J. Power Sources 81 (1999) 67–72.
[6] J. Song, D.W. Shin, Y. Lu, C.D. Amos, A. Manthiram, J.B. Goodenough, Chem. Mater. 24 (2012) 3101–3109.
[7] J. Cabana, M. Casas-Cabanas, F.O. Omenya, N.A. Chernova, D. Zeng, M.S. Whittingham, C.P. Grey, Chem. Mater. 24 (2012) 2952–2964.
[8] J. Xiao, X. Chen, P.V. Sushko, M.L. Sushko, L. Kovarik, J. Feng, Z. Deng, J. Zheng, G.L. Graff, Z. Nie, D. Choi, J. Liu, J.-G. Zhang, M.S. Whittingham, Adv. Mater. 24 (2012) 2109–2116.
[9] X.H. Ma, B. Kang, G. Ceder, J. Electrochem. Soc. 157 (2010) A925–A931.
[10] H.-W. Lee, P. Muralidharan, C.M. Mari, R. Ruffo, D.K. Kim, J. Power Sources 196 (2011) 10712–10716.
[11] H.L. Wang, H. Xia, M.O. Lai, L. Lu, Electrochem. Commun. 11 (2009) 1539–1542.
[12] D. Aurbach, B. Markovsky, Y. Talyossef, G. Salitra, H.J. Kim, S. Choi, J. Power Sources 162 (2006) 780–789.
[13] J. Liu, A. Manthiram, Chem. Mater. 21 (2009) 1695–1707.
[14] H. Duncan, Y. Abu-Lebdeh, I.J. Davidson, J. Electrochem. Soc. 157 (2010) A528–A535.
[15] R. Dedryvere, D. Foix, S. Franger, S. Patoux, L. Daniel, D. Gonbeau, J. Phys. Chem. C 114 (2010) 10999–11008.
[16] Y.K. Sun, C.S. Yoon, I.H. Oh, Electrochim. Acta 48 (2003) 503–506.
[17] J.C. Arrebola, A. Caballero, L. Hernan, J. Morales, J. Power Sources 195 (2010) 4278–4284.
[18] J.Y. Shi, C.W. Yi, K. Kim, J. Power Sources 195 (2010) 6860–6866.
[19] H.M. Wu, I. Belharouak, A. Abouimrane, Y.K. Sun, K. Amine, J. Power Sources 195 (2010) 2909–2913.
[20] D. Liu, Y. Bai, S. Zhao, W. Zhang, J. Power Sources 219 (2012) 333–338.
[21] Y. Huang, J. Chen, J. Ni, H. Zhou, X. Zhang, J. Power Sources 188 (2009) 538–545.
[22] Y. Huang, J. Chen, F. Cheng, W. Wan, W. Liu, H. Zhou, X. Zhang, J. Power Sources 195 (2010) 8267–8274.
[23] J. Lu, Q. Peng, W. Wang, C. Nan, L. Li, Y. Li, J. Am. Chem. Soc. 135 (2013) 1649–1652.
[24] Y.S. Jung, A.S. Cavanagh, L.A. Riley, S.-H. Kang, A.C. Dillon, M.D. Groner, S.M. George, S.-H. Lee, Adv. Mater. 22 (2010) 2172–2176.
[25] M. Kunduraci, G.G. Amatucci, J. Electrochem. Soc. 153 (2006) A1345–A1352.
[26] J.H. Kim, S.T. Myung, C.S. Yoon, S.G. Kang, Y.K. Sun, Chem. Mater. 16 (2004) 906–914.
[27] C. Julien, S. Ziolkiewicz, M. Lemal, M. Massot, J. Mater. Chem. 11 (2001) 1837–1842.
[28] L. Xiao, Y. Zhao, Y. Yang, Y. Cao, X. Ai, H. Yang, Electrochim. Acta 54 (2008) 545–550.
[29] M. Kunduraci, J.F. Al-Sharab, G.G. Amatucci, Chem. Mater. 18 (2006) 3585–3592.
[30] T.F. Yi, X.G. Hu, K. Gao, J. Power Sources 162 (2006) 636–643.
[31] Y. Shin, A. Manthiram, Electrochim. Acta 48 (2003) 3583–3592.